crystals

Article

Understanding the Effect of Austempering Temperature on the Crystallographic Features and Mechanical Properties of Low-Carbon Bainitic Steel

Hao Wu [1,2], Jieru Yu [3], Ziqi Wang [3], Guangjie Qi [3], Bai Xiao [4], Bin Hu [3], Shilong Liu [3,*] and Yishuang Yu [3,*]

[1] State Key Laboratory of Clean and Efficient Turbomachinery Power Equipment, Deyang 618000, China
[2] Dongfang Electric Corporation Dongfang Turbine Co., Ltd., Deyang 618000, China
[3] Institute of Phase Transformation and Structure, School of Materials Science and Engineering, Shanghai Jiao Tong University, Shanghai 200240, China
[4] Institute of Materials, School of Materials Science and Engineering, Shanghai University, Shanghai 200444, China
* Correspondence: sliu6@sjtu.edu.cn (S.L.); yuyishuang@sjtu.edu.cn (Y.Y.)

Abstract: The effect of austempering temperature on crystallographic features and mechanical properties is investigated in low-carbon bainitic steel, focusing on the relationship between microstructure and mechanical properties. After isothermal holding at, above, and below martensite start (M_S) temperatures and tempering, a mixed microstructure of martensite/bainite and martensite/austenite (M/A) constituents is obtained. The fraction of M/A constituents increases as the austempering temperature increases, while the density of block boundaries decreases. The instantaneous work hardening rate exhibits continuous decay without a notable transition because of the retained austenite in the M/A constituents. The toughness decreases with increasing austempering temperature, which is related not only to the fraction of M/A constituents but also to the density of block boundaries. Isothermal treatment below the M_S temperature enables the formation of structures with fewer M/A constituents and high-density block boundaries, through which excellent toughness can be achieved.

Keywords: bainitic steel; phase transformation; M/A constituents; grain boundaries; mechanical properties

check for updates

Citation: Wu, H.; Yu, J.; Wang, Z.; Qi, G.; Xiao, B.; Hu, B.; Liu, S.; Yu, Y. Understanding the Effect of Austempering Temperature on the Crystallographic Features and Mechanical Properties of Low-Carbon Bainitic Steel. *Crystals* **2024**, *14*, 1085. https://doi.org/10.3390/cryst14121085

Academic Editor: Mingyi Zheng

Received: 10 November 2024
Revised: 6 December 2024
Accepted: 16 December 2024
Published: 17 December 2024

Copyright: © 2024 by the authors. Licensee MDPI, Basel, Switzerland. This article is an open access article distributed under the terms and conditions of the Creative Commons Attribution (CC BY) license (https://creativecommons.org/licenses/by/4.0/).

1. Introduction

Low-carbon bainitic (LCB) steel is an indispensable structural material in modern industry due to its high strength, high toughness, and good weldability. The mechanical properties of LCB steel are mainly affected by the characteristics of bainitic structures [1]. The bainitic structures are usually tailored through alloying strategies and process control, which can influence bainite transformation and final transformation products [2–6]. For LCB steel with a specific composition, austempering is a promising method to obtain bainitic structures [7]. This process induces bainite or martensite transformation, forming a mixed microstructure consisting of martensite, bainite, and martensite/austenite (M/A) constituents [4].

Numerous attempts have been made to comprehend the influences of austempering parameters (i.e., austempering temperature and time) on microstructure and resultant mechanical properties [7–12]. Among the austempering parameters, the austempering temperature can significantly affect the characteristics of bainitic structures, such as the morphology of bainite and the M/A constituents [3,4,13–15]. Previous studies have reported that the bainitic ferrite and austenite become coarser at higher austempering temperatures [7,13]. Lowering the austempering temperature contributes to reducing the thickness of bainitic ferrite plates [16,17]. A lower austempering temperature can increase the strength of austenite and promote autocatalytic nucleation of bainite [3]. As a result, more V1/V2 variant pairs are generated, thereby forming higher-density block boundaries. Moreover, high austempering temperatures would cause the formation of blocky M/A constituents,

which results from incomplete transformation [18,19]. The fraction of M/A constituents increases as the austempering temperature increases [3,20]. Generally, M/A constituents would increase the probability of crack initiation due to stress concentration and are detrimental to toughness [21–25]. The block boundaries can enhance crack propagation resistance, thus improving toughness [26]. Therefore, understanding the coupling effects of these two aspects on strength and toughness is vital for the development of LCB steel. However, very few studies have been published on this topic, and the microstructure-properties relationship uncovered from a crystallographic perspective remains limited.

This research aims to systematically investigate the effect of austempering temperature on the crystallographic features and mechanical properties of LCB steel. The characteristics of bainitic structures, including crystallographic features and M/A constituents, are examined to unveil the relationships between microstructure and mechanical properties. Moreover, martensitic structures, prepared by rapid continuous cooling transformation, were also characterized for comparison with bainitic structures. The outcome is expected to provide guidance for the design and preparation of LCB steel.

2. Materials and Methods

An industrial plate steel with a thickness of 12 mm was used in the present work, and its chemical composition is Fe-0.11C-0.48Si-1.13Mn-3.23(Ni + Mo)-0.30(Nb + V) (wt.%). Figure 1a shows the time-temperature-transformation (TTT) curve of the steel calculated using JMatPro® software (Version 11, Sente Software, Guildford, UK). The bainite and martensite start (B_S/M_S) temperatures are 562 °C and 378 °C, respectively. Figure 1b displays a schematic overview of the heat treatments. The heat treatments, including direct-quench and austempering treatments, involve two types of transformation: continuous cooling and isothermal transformations. For the direct-quench treatment, the steel was directly quenched in water after being held at 950 °C for 30 min and then tempered at 400 °C for 30 min. The direct-quenched and tempered steel was labeled as A950T. For the austempering treatment, three selected temperatures were used to obtain different microstructures and resultant mechanical responses. After being austenitized at 950 °C for 30 min, the steels were subjected to isothermal holding in a salt bath maintained at 330, 380, and 430 °C for 30 min, respectively, followed by water cooling. Finally, the isothermally treated steels were tempered at 400 °C for 30 min, and the tempered steels were designated as IT330T, IT380T, and IT430T, respectively.

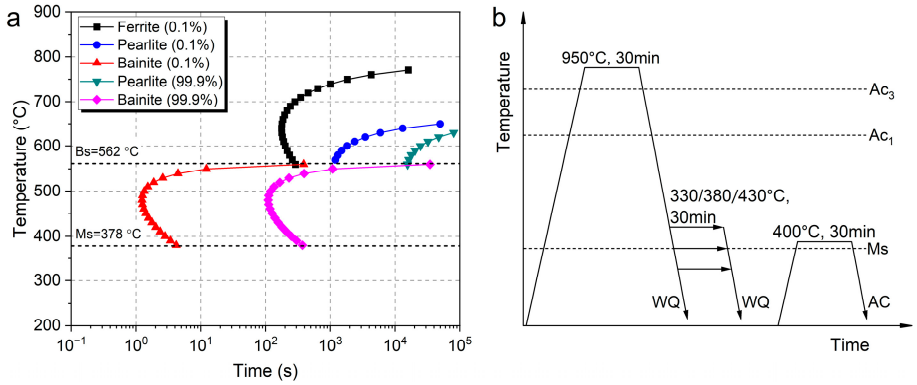


Figure 1. (**a**) calculated TTT curve of the steel, and (**b**) schematic diagram illustrating the heat treatment processes.

After the heat treatments, tensile specimens with gauge dimensions of 15 mm (length) × 5 mm (width) × 1.5 mm (thickness) were cut from the heat-treated steels. The tensile properties were evaluated using a Z100 TEW machine (Zwick/Roell, Ulm, Germany), and the strain rate was 1.0×10^{-3} s^{-1}. Charpy V-notch impact bars were prepared from the transverse orientation of the plates, with dimensions of 10 mm × 10 mm × 55 mm. The

impact test was carried out on a pendulum impact testing machine (PTM2200-D1, Shenzhen, China), with test temperatures ranging from −196 °C to 80 °C. For each condition, three specimens were tested, and their averages were used.

Scanning electron microscopy (SEM) and electron backscatter diffraction (EBSD) techniques were used to obtain morphology. After being mechanically polished and etched with 3 vol.% nital solution, the samples were characterized using a TESCAN MIRA3 FE-SEM (TESCAN, Brno, Czech Republic) to obtain the morphological structures. Additionally, samples were examined using an Oxford Symmetry S3 EBSD detector (Oxford Instruments, Oxford, UK) after being electropolished. HKL Channel 5 software (Oxford Instruments, Oxford, UK) was used to process the EBSD data, and MATLAB® R2017b software (MathWorks, Natick, MA, USA) was utilized to visualize and digitize the crystallographic features.

3. Results

3.1. Mechanical Properties

Figure 2a presents the typical engineering stress-strain curves of the experimental steels, and the tensile properties are summarized in Table 1. As observed in the engineering curves, the yield and ultimate tensile strength of the direct-quenched and tempered steel are significantly higher than those of the isothermally treated and tempered steels. In contrast, the uniform and total elongations of the direct-quenched and tempered steel are lower. For the isothermally treated and tempered steels, the differences in strength and elongation are relatively small.

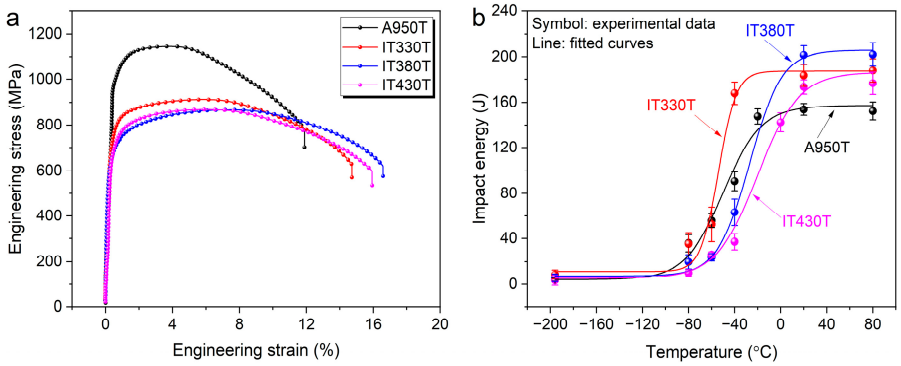


Figure 2. Mechanical properties of the steels: (**a**) engineering stress-strain curves and (**b**) Charpy impact energy plotted as a function of test temperature.

Table 1. Mechanical properties of the steels.

Steel	YS (MPa)	UTS (MPa)	UEL (%)	TEL (%)	LSE (J)	USE (J)	DBTT (°C)
A950T	1021	1146	3.9	11.9	4	157	−50
IT330T	793	913	6.0	14.7	9	187	−54
IT380T	735	868	7.5	16.6	6	205	−27
IT430T	749	869	6.2	15.9	3	185	−21

Note: YS—yield strength, UTS—ultimate tensile strength, UEL—uniform elongation, TEL—total elongation, LSE—lower shelf energy, USE—upper shelf energy, DBTT—ductile-brittle transition temperature.

Figure 2b displays the Charpy impact energy at various temperatures for the steels and fitted curves of the impact energy based on the Boltzmann function. The coefficients of determination of the fitted curves are ~0.99. The upper and lower shelf energies (USE/LSE) are determined as the average impact energies obtained above 20 °C and below −80 °C, respectively. As shown in Table 1, the USEs of A950T, IT330T, IT380T, and IT430T steels are 157, 187, 205, and 185 J, respectively, while these steels have virtually identical LSE. The differences in impact energy become increasingly significant with decreasing test temperature. All the steels exhibit the classic phenomenon of ductile-to-brittle transition with decreasing

test temperature. Thus, the ductile-brittle transition temperature (DBTT), estimated as a temperature corresponding to half of the sum of the USE and LSE, was used to evaluate toughness. The DBTT values of A950T, IT330T, IT380T, and IT430T steels are −50, −54, −27, and −21 °C, respectively. The A950T and IT330T steels exhibit superb toughness compared to the IT380T and IT430T steels. Moreover, the toughness of the isothermally treated and tempered steels decreases with increasing austempering temperature.

3.2. Morphological Structures

Figure 3 shows the SEM micrographs of the steels. In the direct-quenched and tempered steel, the microstructure is a typical lath structure consisting of martensite (M) and lath bainite (LB). The lath boundaries are ambiguous and are decorated with fine and dispersed carbides. For the isothermally treated and tempered steels, the structures are composed of martensite/bainite and M/A constituents, showing characteristics of incomplete transformation, which is consistent with the report in Ref. [3]. In addition, bright and fine carbides are observed in the matrix. In the IT330T steel, the structures are mainly M and LB, accompanied by some fine M/A constituents. As the austempering temperature increases to 380 °C, the microstructure shifts to LB and granular bainite (GB), and the M/A constituents become larger. When the austempering temperature further increases to 430 °C, the IT430T steel shows GB with larger M/A constituents, and the M/A constituent fraction markedly increases. Obviously, the austempering temperature significantly affects the characteristics of bainitic structures.

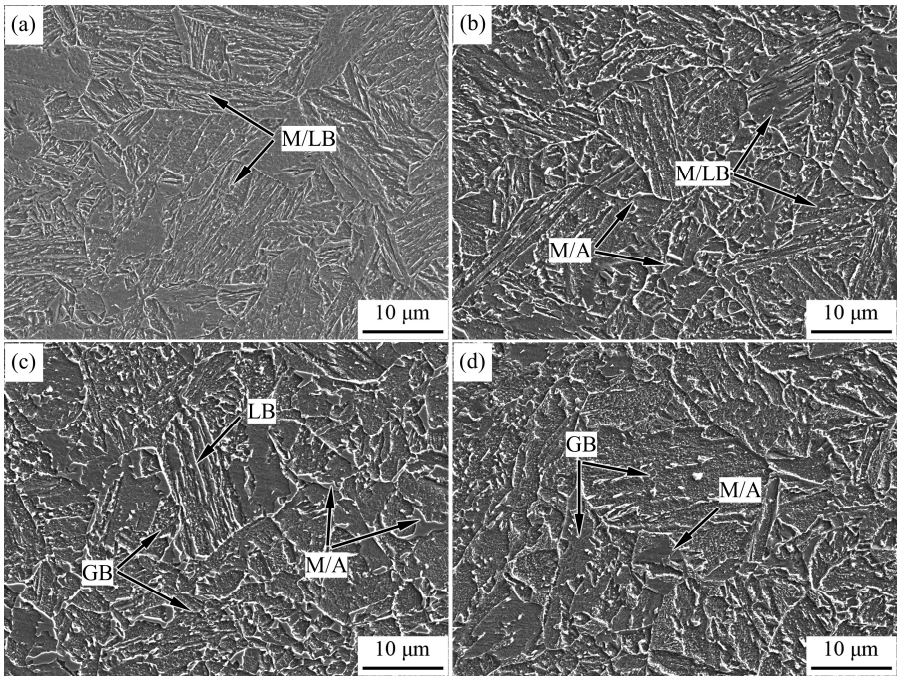


Figure 3. SEM micrographs of the steels: (**a**) A950T, (**b**) IT330T, (**c**) IT380T, and (**d**) IT430T. M: martensite, LB/GB: lath/granular bainite, M/A: martensite/austenite.

3.3. Crystallographic Features

The band contrast (BC) maps, overlapped with phase distribution depicting the microstructure morphology of the steels, are shown in Figure 4. The body-centered cubic and face-centered cubic (bcc and fcc) phases are colored gray and red, respectively. no retained austenite (RA, fcc) was observed in the direct-quenched and tempered steel. In contrast, some RA is detected in the isothermally treated and tempered steels. The volume fraction of RA in IT330T, IT380T, and IT430T steels is 2.50%, 3.57%, and 0.18%, respectively. This indicates that the IT330T and IT380T steels exhibit a higher volume fraction of RA than the IT430T steels. Moreover, some dark regions with low band contrast values are

observed near the RA or at the prior austenite grain boundaries (PAGBs). These regions are reported to be fresh martensite [27], which formed during cooling after the isothermal holding due to the insufficient stability of austenite. The newly formed fresh martensite can cause lattice distortions in the network, which makes it difficult to obtain a good Kikuchi pattern and thus results in a low band contrast value [28]. The RA exists in conjunction with fresh martensite, which together form the M/A constituents. The volume fraction of fresh martensite increases in the isothermally treated and tempered steels with increasing austempering temperature, and so does the volume fraction of M/A constituents.

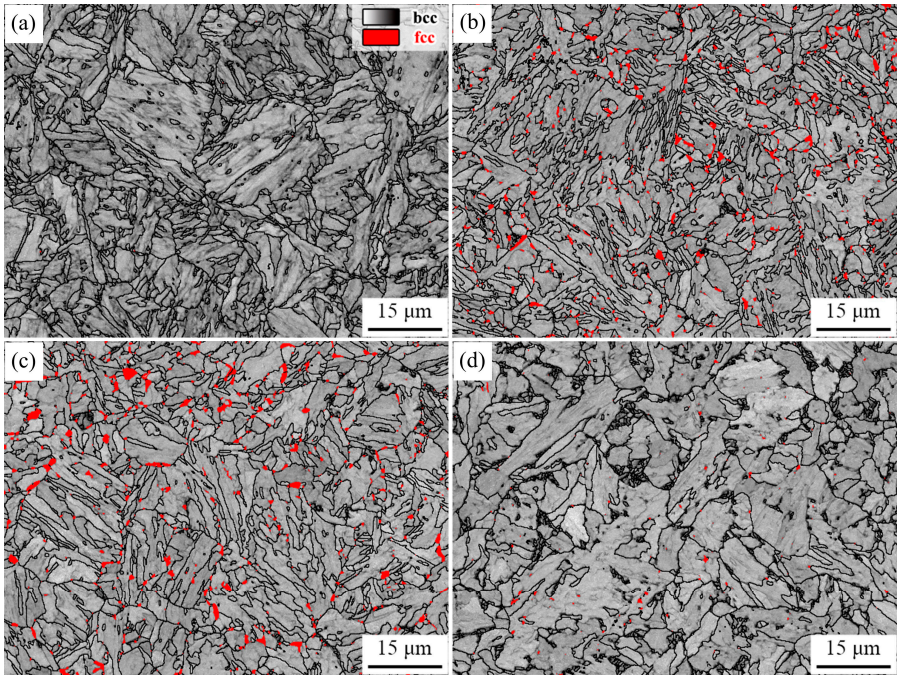


Figure 4. Band contrast (BC) maps overlapped with phase distribution depicting the microstructure morphology of the steels: (**a**) A950T, (**b**) IT330T, (**c**) IT380T, and (**d**) IT430T.

Figure 5 displays the inverse pole figures of the steels. As indicated by the inset stereographic triangle, the crystallographic units with orientations perpendicular to the observed plane are highlighted with particular colors. The regions separated by boundaries with misorientation angles (θ) greater than 15° (black lines) are considered the equivalent effective grains (EGS) [29]. The effective grain sizes (EGS) of A950T, IT330T, IT380T, and IT430T steels are 2.12 ± 3.21, 1.61 ± 2.35, 1.69 ± 2.30, and 1.97 ± 3.39 μm, respectively. Thus, the direct-quenched and tempered steel exhibits a larger EGS than the isothermally treated and tempered steels, and the IT330T steel shows the finest EGS among the studied steels.

Figure 6 presents the band contrast maps with boundary distribution of the steels. Here, black and red lines represent the high -angle grain boundaries (HAGBs, $\theta > 15°$). The densities of HAGBs ($15° < \theta < 45°$) are almost the same, while the densities of HAGBs ($\theta > 45°$) differ. The densities of HAGBs ($\theta > 45°$) in A950T, IT330T, IT380T, and IT430T steels are 0.83, 1.05, 0.81, and 0.64 μm^{-1}, respectively. The density of HAGBs ($\theta > 45°$) in the isothermally treated and tempered steels decreases with increasing austempering temperature. Moreover, most of the HAGBs ($\theta > 45°$) are straight in IT330T and IT380T steels, while they are curved in A950T and IT430T steels. The density and morphology of boundaries result from variant selection, which will be discussed in Section 4.1.

Figure 7 shows the Kernel average misorientation (KAM) maps of the steels. The maps reflect the distribution of geometrically necessary dislocations (GND) [30]. The areas with high KAM values in A950T and IT330T steels are larger than those in IT380T and IT430T steels, implying a higher GND density in the A950T and IT330T steels. In the isothermally

treated and tempered steels, the areas with high KAM values decrease with increasing austempering temperature, indicating a tendency for the GND density to decrease.

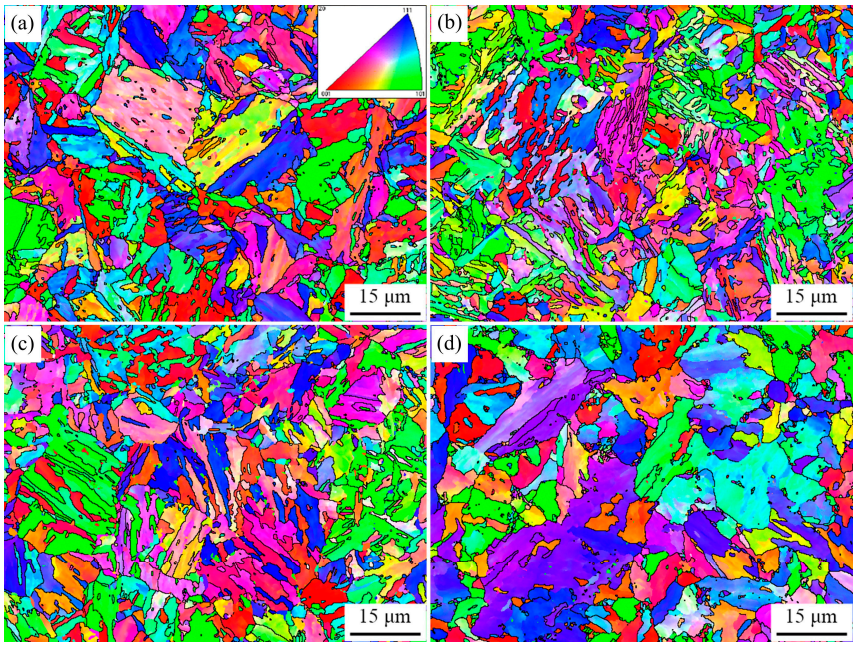


Figure 5. Inverse pole figures of the steels: (**a**) A950T, (**b**) IT330T, (**c**) IT380T, and (**d**) IT430T.

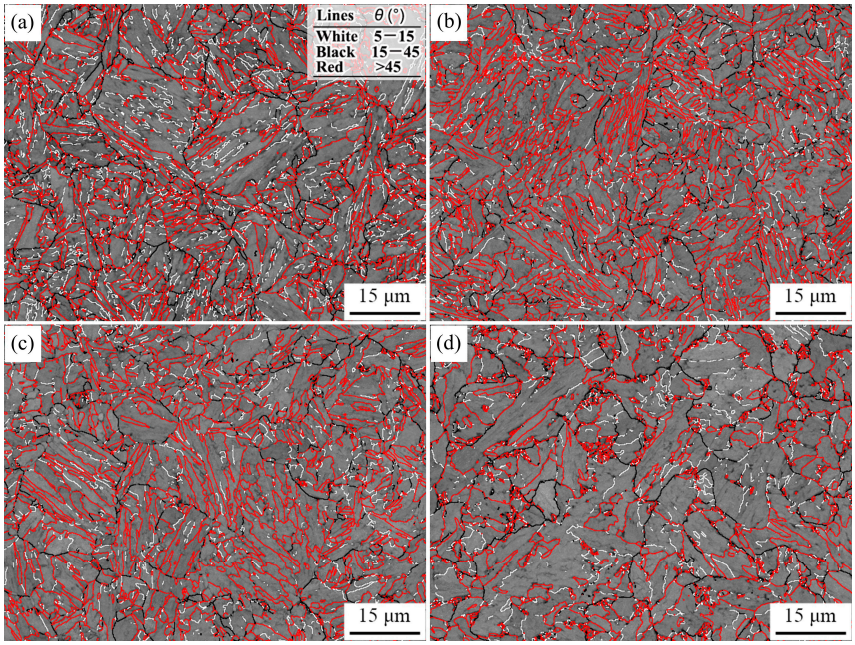


Figure 6. Band contrast maps with boundary distribution of the steels: (**a**) A950T, (**b**) IT330T, (**c**) IT380T, and (**d**) IT430T.

Figure 8 shows the quantitatively calculated results based on Figures 4–7. The volume fraction of M/A constituents in the A950T, IT330T, IT380T, and IT430T steels is 0.02%, 4.99%, 6.44%, and 10.22%, respectively. In the isothermally treated and tempered steels, the volume fraction of M/A constituents increases with increasing austempering temperature. Moreover, the EGS increases as the austempering temperature increases, while the density of HAGBs ($\theta > 45°$) decreases. It is inferred that lowering the austempering temperature contributes to the refinement of the structures. The GND density was calculated based on

the KAM map. As shown in Figure 8d, the curves of GND density from left to right are IT430T, IT380T, IT330T, and A950T. This suggests that the value of GND density follows the sequence: IT430T < IT380T < IT330T < A950T.

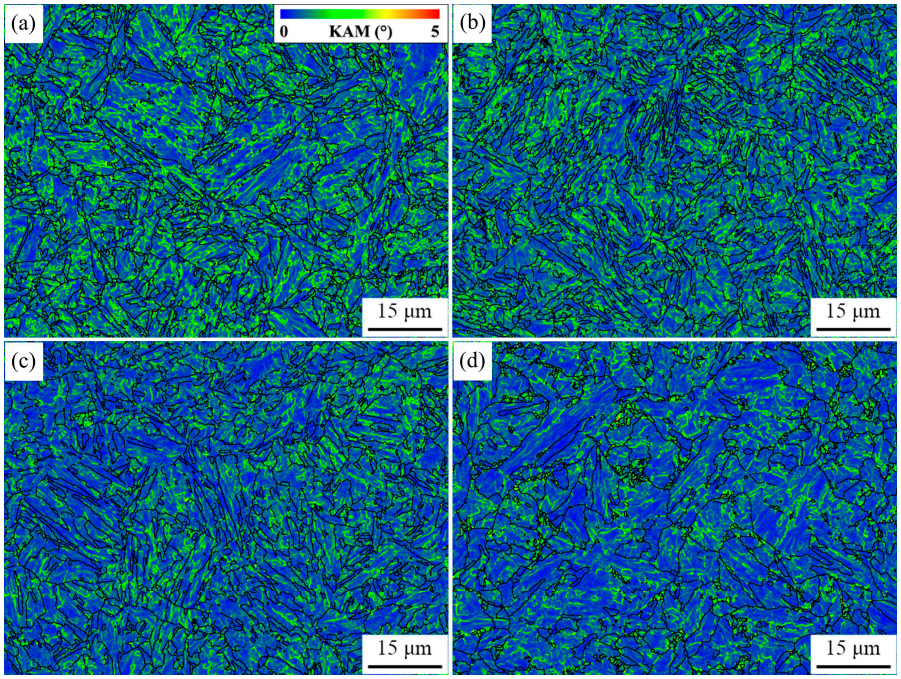


Figure 7. Kernel average misorientation maps of the steels: (**a**) A950T, (**b**) IT330T, (**c**) IT380T, and (**d**) IT430T.

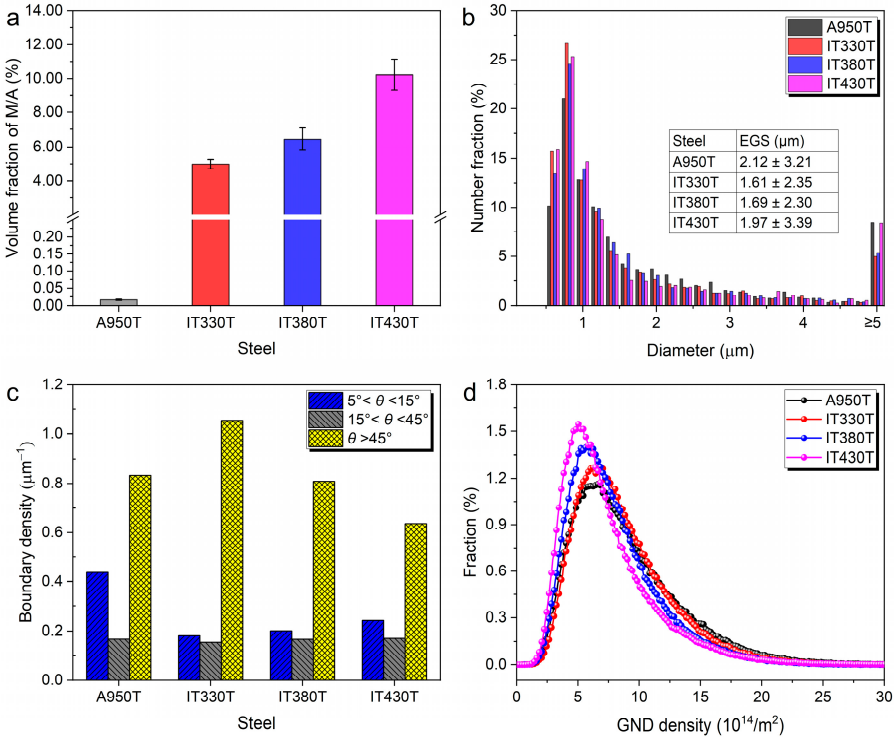


Figure 8. Volume fraction of M/A constituents (**a**), grain size distribution (**b**), boundary density (**c**) and GND density (**d**) of the steels.

4. Discussion

4.1. Digitization and Visualization of the Crystallographic Features

The crystallographic features result from variant selection [31–35]. In general, there are 24 possible variants holding the Kurdjumov-Sachs (K-S) orientation relationship in low-carbon steels [32]. When V1 is used as a reference, 16 distinct variant pairs are generated due to the interaction between the possible variants [13]. In the present study, the orientation relationship (OR) between parent austenite and product variants for the steels was calculated using numerical fitting calculations [36]. The ORs of A950T, IT330T, IT380T, and IT430T steels were determined to be (118.4°, 8.5°, 197.6°), (122.8°, 8.9°, 193.7°), (120.7°, 8.8°, 195.6°), and (120.8°, 8.6°, 195.7°), respectively. Based on the actual OR, the density of intervariant boundaries between V1 and other variants was calculated.

Figure 9 depicts the density of intervariant boundaries in the steels. Most intervariant boundaries come from the variants within the same crystallographic packet group (i.e., CP1), with V1/V2 variant pairs being predominant. Based on the boundary types, the intervariant boundaries can be further divided into block, sub-block, and packet boundaries [13,32]. It is evident that the IT330T and IT380T steels show a significantly higher density of block boundaries than the A950T and IT430T steels. In the isothermally treated and tempered steels, the density of block boundaries decreases as the austempering temperature increases, as does the density of V1/V2 variant boundaries. Previous studies indicate that V1/V2 boundaries are block boundaries and usually appear in a straight shape [37]. Therefore, it can be inferred that the straight boundaries ($\theta > 45°$) in IT330T and IT380T steels are mainly from V1/V2 variant pairs. Lowering the austempering temperature contributes to forming more V1/V2 variant pairs.

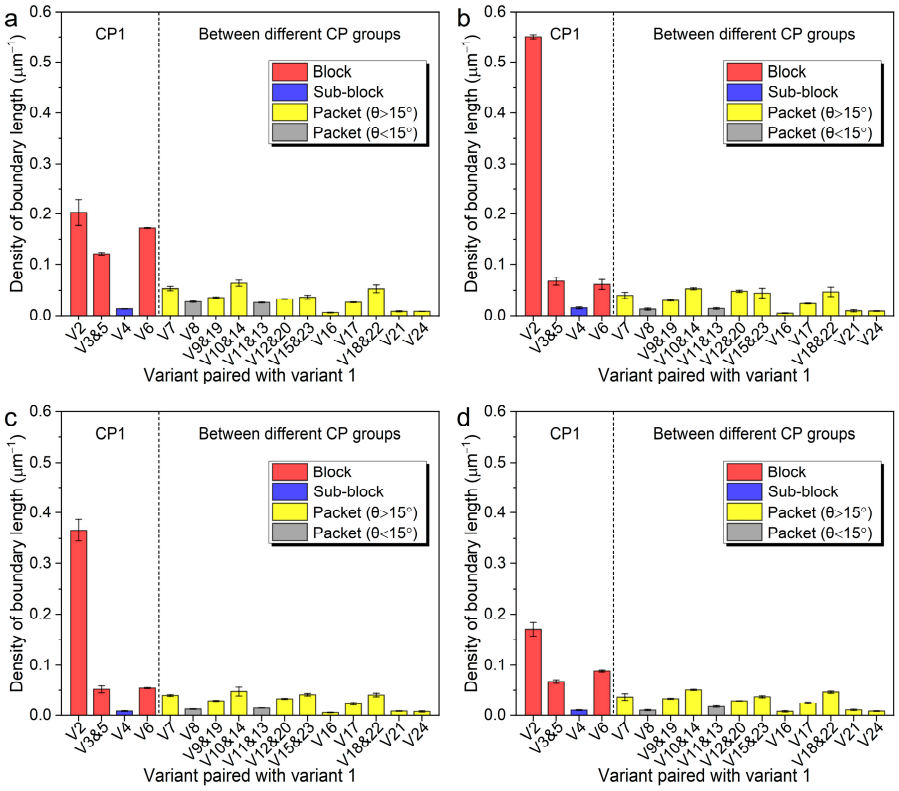


Figure 9. Density of intervariant boundaries of the steels: (**a**) A950T, (**b**) IT330T, (**c**) IT380T, and (**d**) IT430T.

The variant pairing behavior of the steels is schematically illustrated in Figure 10. The figure shows the schematics of the heat treatment processes and crystallographic features of the steels depending on continuous cooling and isothermal transformation. In the

schematic grains (Figure 10b), the region that contains variants from the same Bain group is depicted by identical colors. The same CP group shows characteristics in which the region is composed of Bain groups with the same elongated direction. The variant pairing behavior can be classified into four types. As shown in Figure 10a, the direct-quenched and tempered steel forms a mixed microstructure of M and LB due to continuous cooling transformation, and the crystallographic features are depicted in Figure 10b. The variants of the same CP group are formed side by side, and no RA is observed (Type I). For the isothermally treated and tempered steels, the microstructure contains M/A constituents, showing characteristics of incomplete transformation. When the steel is isothermally treated below the M_S temperature, the structure is M and LB with some fine M/A constituents (type II). The variants sharing the same CP group are generated, and the dominant variant pairing is the V1/V2 pair. As the austempering temperature increases to the M_S temperature, the microstructure becomes LB and GB, with larger M/A constituents (type III). The variant pairing behavior at this temperature exhibits similar characteristics to type II. But unlike type II, the schematic grain of type III has larger M/A constituents. As the steel is isothermally treated above the M_S temperature, the microstructure is mainly GB, and the matrix is decorated with larger M/A constituents (type IV). Variants of the same Bain group are preferred adjacently, resulting in the formation of coarse Bain zones. Clearly, the degree of incomplete bainite transformation decreases with decreasing austempering temperature, and the microstructure becomes finer.

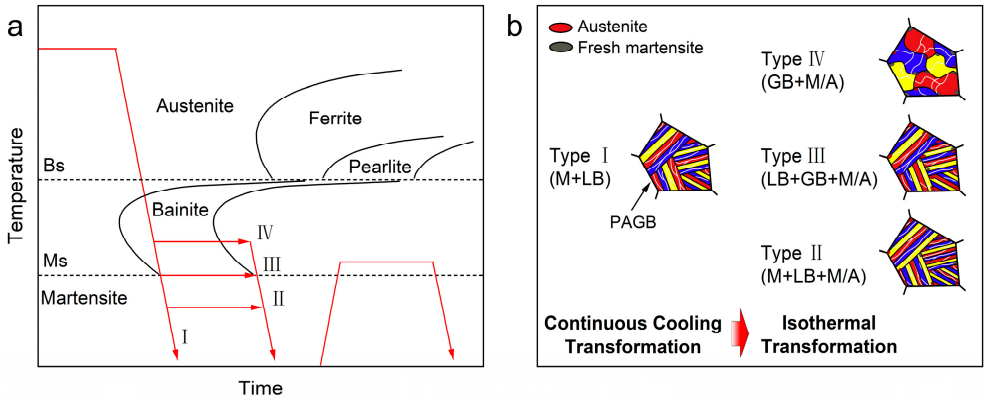


Figure 10. Schematics illustrating the heat treatment processes (**a**) and crystallographic features (**b**) of the steels depending on continuous cooling and isothermal transformation. In the schematic grains, white and black lines stand for low and high angle boundaries, respectively. I, II, III and IV represent the processes of direct quenching and tempering, as well as isothermal holding below, at, and above M_S temperatures and tempering, respectively, and corresponding types of crystallographic features.

Previous studies have shown that the variation in variant pairing with isothermal temperature is associated with the driving force for transformation and self-accommodation of transformation strain [2,38]. As the isothermal temperature decreases, the driving force for bainite transformation increases. Accordingly, variant selection becomes weaker, which induces the formation of more variants and finer transformation products [3]. Moreover, self-accommodation of transformation strain through the formation of distinct variants in the neighbors is enhanced due to the strengthened austenite from lowering the isothermal temperature [17]. In the current work, the variant pairing behavior changes from type IV to type III and finally to type II as the austempering temperature lowers and the driving force increases. The coarse bainitic structures of type IV are likely to form at a smaller driving force and higher austempering temperature, while the lath bainitic structures of type II are preferentially formed at a larger driving force and lower austempering temperature. A lower austempering temperature and larger driving force can trigger the formation of more variants from distinct Bain groups and thus increase the density of HAGBs.

4.2. Strength and Strain Hardening Behavior

For a better understanding of the yielding behavior of the studied steels, the extended Kocks-Mecking (K-M) curves are used in the current analysis. The K-M curve, which shows the instantaneous work hardening rate (Θ, $d\sigma/d\varepsilon$) as a function of true stress, has been validated as a reliable method for determining the yield stress of steels [39]. In general, the curves exhibit the same shape and can be separated into two stages before uniform elongation is exceeded [40]. In the first stage (stage I), due to the bowing of matrix dislocations, Θ drops gradually with anelastic reversible behavior. In the second stage (stage II), Θ decays further with a marked transition to the plastic regime due to massively multiply dislocations.

Figure 11 shows the extended K-M curves of the steels. The transitions, highlighted with black, red, blue, and pink dots, represent the yielding of the A950T, IT330T, IT380T, and IT430T steels, respectively. The direct-quenched and tempered steel exhibits a clear transition between stage I and stage II, marked by a black dot. The yielding behavior can be attributed to the diminishing of dislocation mobility caused by carbide precipitation and dislocation recovery in the matrix after tempering [41]. On the contrary, the isothermally treated and tempered steels show a continuous decrease in Θ without a notable transition, indicating continuous yielding. This might be related to the M/A constituents, in which the RA in the M/A constituents can yield at a lower stress level compared with the martensite/bainite [42]. As a result, the initial yielding and subsequent work hardening behavior are modified compared with the direct-quenched and tempered steel.

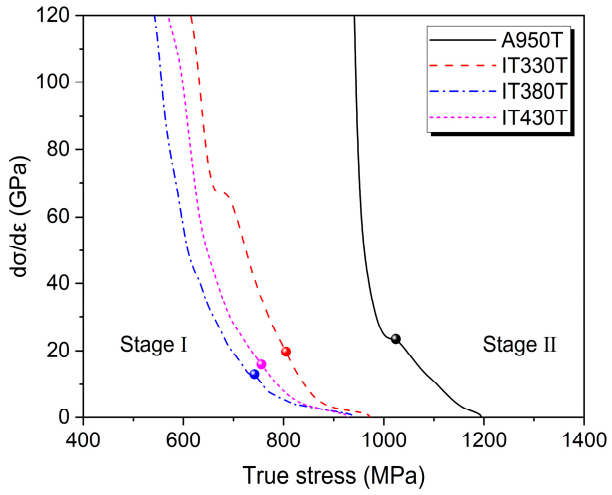


Figure 11. Extended K-M curves of the studied steels. The transition marked by dots representing the yield strength.

4.3. Correlation of Crystallographic Features and Toughness

To reveal the relationship between crystallographic features and toughness, the density of intervariant boundaries was summarized. The densities of block, sub-block, and packet boundaries are shown in Figure 12a, along with the corresponding DBTT of the studied steels. The four steels exhibit almost the same densities of sub-block and packet boundaries, but their densities of block boundaries are significantly different. Moreover, an interesting phenomenon is observed in the density of block boundaries, which shows a strong correlation with the DBTT. Namely, the steel with a higher density of block boundaries has a lower DBTT, indicating that the steel has better toughness. Previous studies have demonstrated that HAGBs dominated by block boundaries can effectively hinder crack propagation, thus improving toughness [43–45]. Therefore, it is inferred that the block boundary is one of the key factors affecting toughness in the current work.

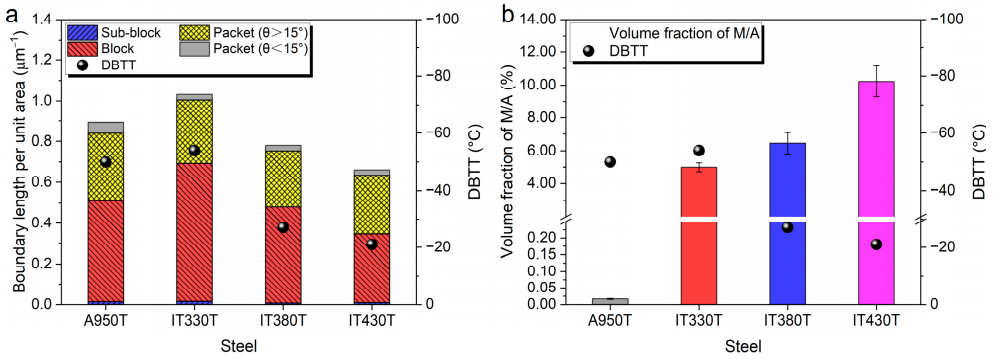


Figure 12. Relationship between crystallographic features and toughness of the steels: (**a**) boundary density vs. toughness, (**b**) M/A fraction vs. toughness.

Another interesting phenomenon is that the IT380T steel has almost the same density of block boundaries as the A950T steel, yet it exhibits a higher DBTT, suggesting poorer toughness. This observation indicates the existence of other factors that affect toughness in this work. The intriguing and counter-intuitive phenomenon might be associated with the M/A constituents resulting from the incomplete austenite-bainite transformation [37]. Figure 12b shows the relationship between the volume fraction of M/A constituents and the corresponding DBTT of the steels. It is evident that the isothermally treated and tempered steels exhibit a higher volume fraction of M/A constituents compared with the direct-quenched and tempered steel, showing significant incomplete phase transformation characteristics. The M/A constituents are transformed from austenite with high carbon concentration and have high hardness [22,46], which could promote the initiation of cleavage cracks and deteriorate toughness [21,23,47–50]. In the current work, the IT380T steel has a larger amount of M/A constituents than the A950T steel, with roughly equal density of block boundaries, yet weaker toughness. This suggests that the negative effect of M/A constituents on toughness is significantly greater than the positive impact of the block boundaries.

Based on the above analysis, the toughness of the isothermally treated and tempered steels is the result of "double effects." One effect results from the M/A constituents, which promote the initiation of cleavage cracks and deteriorate toughness. The other results from the block boundaries, which can effectively deflect or arrest crack propagation and contribute to toughness. Hence, it is concluded that a structure with high-density block boundaries and fewer M/A constituents helps achieve superb toughness. In this study, the ideal structure with excellent toughness can be obtained through isothermal holding at temperatures below M_S.

5. Conclusions

The effect of austempering temperature on crystallographic features and mechanical properties of low-carbon bainitic steel was investigated, and the microstructure-properties relationship was discussed in detail. The main conclusions are as follows:

(1) The isothermally treated and tempered steels exhibit a mixed microstructure of martensite/bainite and M/A constituents, showing significant incomplete phase transformation characteristics. The fraction of M/A constituents increases with increasing austempering temperature. Moreover, the density of block boundaries decreases as the austempering temperature increases, along with a reduced density of V1/V2 variant boundaries.

(2) The yielding behavior of the isothermally treated and tempered steels was analyzed using extended Kocks-Mecking plots. The RA in the M/A constituents can yield at a lower stress level than martensite/bainite, leading to a continuous decay of the instantaneous work hardening rate without a notable transition.

(3) The DBTT of the isothermally treated and tempered steels decreases as the austempering temperature increases, resulting from the coupling effects of M/A constituents and block boundaries. The microstructure obtained through isothermal holding at temperatures below M_S has fewer M/A constituents and high-density block boundaries, contributing to improved toughness.

Author Contributions: Conceptualization, S.L. and Y.Y.; methodology, S.L. and Y.Y.; software, Y.Y.; validation, H.W., S.L. and Y.Y.; formal analysis, H.W., S.L. and Y.Y.; investigation, H.W., J.Y., Z.W., G.Q., B.X. and B.H.; resources, H.W.; data curation, Y.Y.; writing—original draft preparation, H.W. and Y.Y.; writing—review and editing, J.Y., Z.W., G.Q., B.X. and B.H.; visualization, H.W. and Y.Y.; supervision, S.L. and Y.Y.; project administration, S.L.; funding acquisition, S.L. and Y.Y. All authors have read and agreed to the published version of the manuscript.

Funding: This research was funded by the China Postdoctoral Science Foundation (No. 2023M732192) and the National Natural Science Foundation of China (No. 52101045).

Data Availability Statement: The data presented in this study are available on request from the corresponding author due to legal and ethical reasons.

Conflicts of Interest: H.W. was employed by the State Key Laboratory of Clean and Efficient Turbomachinery Power Equipment and the Dongfang Electric Corporation Dongfang Turbine Co., Ltd. The remaining authors declare that the research was conducted in the absence of any commercial or financial relationships that could be construed as a potential conflict of interest.

References

1. Bhadeshia, H.K.D.H.; Honeycombe, R.W.K. *Steels: Microstructure and Properties*, 4th ed.; Butterworth-Heinemann: Oxford, UK, 2017.
2. Kawata, H.; Sakamoto, K.; Moritani, T.; Morito, S.; Furuhara, T.; Maki, T. Crystallography of ausformed upper bainite structure in Fe–9Ni–C alloys. *Mater. Sci. Eng. A* **2006**, *438–440*, 140–144. [CrossRef]
3. Wu, B.; Zhou, T.; Wang, Z.; Wang, X.; Shang, C.; Yu, Y.; Elhefnawey, M.; Li, L. Effects of carbon concentration and transformation temperature on incomplete transformation and crystallography of low-carbon bainitic steel. *J. Mater. Res. Technol.* **2024**, *32*, 827–840. [CrossRef]
4. Yao, C.; Lan, H.; Tao, Z.; Qi, M.; Du, L. Microstructure, crystallography, mechanical and damping properties of a low-carbon bainitic steel austempered at various temperatures. *J. Mater. Sci.* **2022**, *57*, 19068–19087. [CrossRef]
5. Guo, H.; Gao, X.; Bai, Y.; Enomoto, M.; Yang, S.; He, X. Variant selection of bainite on the surface of allotriomorphic ferrite in a low carbon steel. *Mater. Charact.* **2012**, *67*, 34–40. [CrossRef]
6. Zhao, L.; Qian, L.; Zhou, Q.; Li, D.; Wang, T.; Jia, Z.; Zhang, F.; Meng, J. The combining effects of ausforming and below-Ms or above-Ms austempering on the transformation kinetics, microstructure and mechanical properties of low-carbon bainitic steel. *Mater. Des.* **2019**, *183*, 108123. [CrossRef]
7. Putatunda, S.K.; Martis, C.; Boileau, J. Influence of austempering temperature on the mechanical properties of a low carbon low alloy steel. *Mater. Sci. Eng. A* **2011**, *528*, 5053–5059. [CrossRef]
8. Furuhara, T.; Kawata, H.; Morito, S.; Miyamoto, G.; Maki, T. Variant selection in grain boundary nucleation of upper bainite. *Metall. Mater. Trans. A* **2008**, *39*, 1003–1013. [CrossRef]
9. Hu, H.; Imed-Eddine, B.; Xu, G.; Tian, J.; Zhou, M.; Bréchet, Y.; Zurob, H.S. Effect of temperature, carbon content and crystallography on the lengthening kinetics of bainitic ferrite laths. *Mater. Charact.* **2022**, *187*, 111860. [CrossRef]
10. Bhuyan, D.; Sastry, G.V.S.; Patra, S.; Pradhan, S.K.; Manna, R. Effect of austempering time on bainite plate thickness and variant selection in a high carbon low alloy steel. *Mater. Charact.* **2023**, *200*, 112923. [CrossRef]
11. Wang, K.; Hu, F.; Zhou, W.; Zhang, D.; Yin, C.; Yershov, S.; Wu, K. Effect of refined multi-scale microstructures on the ultra-high impact toughness of bainitic steel austempered below Ms temperature. *J. Mater. Res. Technol.* **2023**, *26*, 5773–5785. [CrossRef]
12. Sun, D.; Feng, X.; Zhang, P.; Sun, X.; Yang, Z.; Long, X.; Zhang, F. Effects of two-step austempering processes on the wear resistance and fatigue lifetime of high-carbon nanostructured bainitic steel. *J. Mater. Res. Technol.* **2024**, *30*, 4739–4749. [CrossRef]
13. Takayama, N.; Miyamoto, G.; Furuhara, T. Effects of transformation temperature on variant pairing of bainitic ferrite in low carbon steel. *Acta Mater.* **2012**, *60*, 2387–2396. [CrossRef]
14. Mondal, J.; Das, K.; Das, S. Isothermal transformation kinetics, microstructure and mechanical properties of a carbide free bainitic steel. *Mater. Charact.* **2021**, *177*, 111166. [CrossRef]
15. Ståhlkrantz, A.; Hedström, P.; Sarius, N.; Borgenstam, A. Influence of austempering conditions on hardness and microstructure of bainite in low-alloyed steel. *Metall. Mater. Trans. A* **2024**, *55*, 209–217. [CrossRef]
16. Garcia-Mateo, C.; Paul, G.; Somani, M.C.; Porter, D.A.; Bracke, L.; Latz, A.; Garcia De Andres, C.; Caballero, F.G. Transferring nanoscale bainite concept to lower C contents: A perspective. *Metals* **2017**, *7*, 159. [CrossRef]

17. Yu, Y.; Zhao, J.; Wang, X.; Guo, H.; Xie, Z.; Shang, C. Unraveling the significance of cobalt on transformation kinetics, crystallography and impact toughness in high strength steels. *Int. J. Miner. Metall. Mater.* **2024**, *32*, 1–11. [CrossRef]
18. Aaronson, H.I.; Reynolds, W.T.; Purdy, G.R. The incomplete transformation phenomenon in steel. *Metall. Mater. Trans. A* **2006**, *37*, 1731–1745. [CrossRef]
19. Bhadeshia, H.K.D.H.; Christian, J.W. Bainite in steels. *Metall. Trans. A* **1990**, *21*, 767–797. [CrossRef]
20. Chang, L.C.; Bhadeshia, H.K.D.H. Austenite films in bainitic microstructures. *Mater. Sci. Technol.* **1995**, *11*, 874–882. [CrossRef]
21. Mohseni, P.; Solberg, J.K.; Karlsen, M.; Akselsen, O.M.; Østby, E. Cleavage fracture initiation at M–A constituents in intercritically coarse-grained heat-affected zone of a HSLA steel. *Metall. Mater. Trans. A* **2014**, *45*, 384–394. [CrossRef]
22. Li, X.; Shang, C.; Ma, X.; Gault, B.; Subramanian, S.V.; Sun, J.; Misra, R.D.K. Elemental distribution in the martensite–austenite constituent in intercritically reheated coarse-grained heat-affected zone of a high-strength pipeline steel. *Scr. Mater.* **2017**, *139*, 67–70. [CrossRef]
23. Lan, L.; Qiu, C.; Song, H.; Zhao, D. Correlation of martensite–austenite constituent and cleavage crack initiation in welding heat affected zone of low carbon bainitic steel. *Mater. Lett.* **2014**, *125*, 86–88. [CrossRef]
24. Fujita, N.; Ishikawa, N.; Roters, F.; Tasan, C.C.; Raabe, D. Experimental–numerical study on strain and stress partitioning in bainitic steels with martensite–austenite constituents. *Int. J. Plast.* **2018**, *104*, 39–53. [CrossRef]
25. Li, Y.; Baker, T.N. Effect of morphology of martensite-austenite phase on fracture of weld heat affected zone in vanadium and niobium microalloyed steels. *Mater. Sci. Technol.* **2010**, *26*, 1029–1040. [CrossRef]
26. Gourgues, A.F. Electron backscatter diffraction and cracking. *Mater. Sci. Technol.* **2002**, *18*, 119–133. [CrossRef]
27. Xiao, B.; Yu, Y.; Hu, B.; Wang, H.; Wang, W.; Liu, S.; Misra, R.D.K.; Liu, W. On balanced strength and ductility synergy in low alloy steels through multiphase heterostructure involving cumulative process of hot rolling, coiling and tempering. *Mater. Sci. Eng. A* **2024**, *891*, 145987. [CrossRef]
28. Petrov, R.; Kestens, L.; Wasilkowska, A.; Houbaert, Y. Microstructure and texture of a lightly deformed TRIP-assisted steel characterized by means of the EBSD technique. *Mater. Sci. Eng. A* **2007**, *447*, 285–297. [CrossRef]
29. Ali, M.; Porter, D.; Kömi, J.; Eissa, M.; El Faramawy, H.; Mattar, T. Characterization of the microstructure and precipitates formed during the thermomechanical processing of a CrNiMoWMnV ultrahigh-strength steel. *Steel Res. Int.* **2020**, *91*, 1900580. [CrossRef]
30. Calcagnotto, M.; Ponge, D.; Demir, E.; Raabe, D. Orientation gradients and geometrically necessary dislocations in ultrafine grained dual-phase steels studied by 2D and 3D EBSD. *Mater. Sci. Eng. A* **2010**, *527*, 2738–2746. [CrossRef]
31. Li, X.C.; Zhao, J.X.; Cong, J.H.; Misra, R.D.K.; Wang, X.M.; Wang, X.L.; Shang, C.J. Machine learning guided automatic recognition of crystal boundaries in bainitic/martensitic alloy and relationship between boundary types and ductile-to-brittle transition behavior. *J. Mater. Sci. Technol.* **2021**, *84*, 49–58. [CrossRef]
32. Morito, S.; Tanaka, H.; Konishi, R.; Furuhara, T.; Maki, T. The morphology and crystallography of lath martensite in Fe-C alloys. *Acta Mater.* **2003**, *51*, 1789–1799. [CrossRef]
33. Zhao, H.T.; Gao, J.H.; Wu, G.L.; Wu, H.H.; Zhang, C.L.; Huang, Y.H.; Wang, S.Z.; Mao, X.P. Variant pairing quantification method for a bainitic HSLA steel. *Metall. Mater. Trans. A* **2023**, *54*, 3697–3702. [CrossRef]
34. Wang, X.; Xie, Z.; Li, X.; Shang, C. Recent progress in visualization and digitization of coherent transformation structures and application in high-strength steel. *Int. J. Miner. Metall. Mater.* **2024**, *31*, 1298–1310. [CrossRef]
35. Zhao, H.T.; Gao, J.H.; Wu, G.L.; Wu, H.H.; Zhang, C.L.; Huang, Y.H.; Luo, Y.; Yang, X.Q.; Wang, S.Z. Crystallographic characteristics of acicular ferrite nucleated on inclusions in a HSLA steel. *J. Mater. Res. Technol.* **2024**, *28*, 1957–1966. [CrossRef]
36. Miyamoto, G.; Takayama, N.; Furuhara, T. Accurate measurement of the orientation relationship of lath martensite and bainite by electron backscatter diffraction analysis. *Scr. Mater.* **2009**, *60*, 1113–1116. [CrossRef]
37. Wang, X.L.; Wang, Z.Q.; Xie, Z.J.; Wang, J.L.; Li, X.C.; Shang, C.J. Toughening coarse grained heat affected zone of high strength offshore engineering steel by enhancing the completeness of austenite-bainite transformation. *Mater. Lett.* **2019**, *257*, 126727. [CrossRef]
38. Furuhara, T.; Kawata, H.; Morito, S.; Maki, T. Crystallography of upper bainite in Fe–Ni–C alloys. *Mater. Sci. Eng. A* **2006**, *431*, 228–236. [CrossRef]
39. Kocks, U.F.; Mecking, H. Physics and phenomenology of strain hardening: The FCC case. *Prog. Mater Sci.* **2003**, *48*, 171–273. [CrossRef]
40. Arechabaleta, Z.; van Liempt, P.; Sietsma, J. Quantification of dislocation structures from anelastic deformation behaviour. *Acta Mater.* **2016**, *115*, 314–323. [CrossRef]
41. Yu, Y.-S.; Hu, B.; Gao, M.-L.; Xie, Z.-J.; Rong, X.-Q.; Han, G.; Guo, H.; Shang, C.-J. Determining role of heterogeneous microstructure in lowering yield ratio and enhancing impact toughness in high-strength low-alloy steel. *Int. J. Miner. Metall. Mater.* **2021**, *28*, 816–825. [CrossRef]
42. Navarro-López, A.; Hidalgo, J.; Sietsma, J.; Santofimia, M.J. Unravelling the mechanical behaviour of advanced multiphase steels isothermally obtained below Ms. *Mater. Des.* **2020**, *188*, 108484. [CrossRef]
43. Yu, Y.-S.; Wang, Z.-Q.; Wu, B.-B.; Zhao, J.-X.; Wang, X.-L.; Guo, H.; Shang, C.-J. Tailoring variant pairing to enhance impact toughness in high-strength low-alloy steels via trace carbon addition. *Acta Metall. Sin. (Engl. Lett.)* **2021**, *34*, 755–764. [CrossRef]
44. Qi, X.; Huan, P.; Wang, X.; Di, H.; Shen, X.; Sun, Q.; Liu, Z.; He, J. Study on the mechanism of heat input on the grain boundary distribution and impact toughness in CGHAZ of X100 pipeline steel from the aspect of variant. *Mater. Charact.* **2021**, *179*, 111344. [CrossRef]

45. Pan, Z.D.; Wang, E.M.; Wu, H.B.; Wu, J.P.; Hong, J.; Liu, Z.Z.; Guo, A.M.; Sun, Z.; Hao, Y.S. Direct quenching and tempering to achieve high strength and toughness of GPa-Grade nano-precipitated steel: The effect of precipitation behavior and variant selectivity. *J. Mater. Res. Technol.* **2024**, *33*, 1140–1154. [CrossRef]
46. Lan, L.; Yu, M.; Qiu, C. On the local mechanical properties of isothermally transformed bainite in low carbon steel. *Mater. Sci. Eng. A* **2019**, *742*, 442–450. [CrossRef]
47. Li, X.; Fan, Y.; Ma, X.; Subramanian, S.V.; Shang, C. Influence of martensite–austenite constituents formed at different intercritical temperatures on toughness. *Mater. Des.* **2015**, *67*, 457–463. [CrossRef]
48. Qi, X.; Di, H.; Wang, X.; Liu, Z.; Misra, R.D.K.; Huan, P.; Gao, Y. Effect of secondary peak temperature on microstructure and toughness in ICCGHAZ of laser-arc hybrid welded X100 pipeline steel joints. *J. Mater. Res. Technol.* **2020**, *9*, 7838–7849. [CrossRef]
49. Li, Y.; Feng, Q.S.; Jia, H.D.; Cui, S.H.; Dai, L.S.; Wu, H.B.; Liu, Q.Y.; Zhang, H.S.; Jia, S.J. Multi-angle analysis of Mo on martensite–austenite component and toughness in SCGHAZ of X80 pipeline automatic ring welding. *J. Mater. Res. Technol.* **2024**, *33*, 115–129. [CrossRef]
50. Nellikode, S.; Murugan, S.P.; Chung, J.-H.; Lee, C.-H.; Park, H.; Kim, S.-D.; Ku, N.; Park, Y.-D. Role of M-A constituents in bainitic microstructure on crack propagation behavior in the ICCGHAZ of HSLA steels for offshore applications. *J. Mater. Res. Technol.* **2024**, *32*, 250–260. [CrossRef]

Disclaimer/Publisher's Note: The statements, opinions and data contained in all publications are solely those of the individual author(s) and contributor(s) and not of MDPI and/or the editor(s). MDPI and/or the editor(s) disclaim responsibility for any injury to people or property resulting from any ideas, methods, instructions or products referred to in the content.